Mechanical Systems and Signal Processing 166 (2022) 108442

Contents lists available at ScienceDirect

Mechanical Systems and Signal Processing

journal homepage: www.elsevier.com/locate/ymssp

Two-phase flow-induced vibration fatigue damage of tube bundles with clearance restriction

Jiang Lai [a,*], Shihao Yang [a], Lingling Lu [b], Tiancai Tan [a], Lei Sun [a]

[a] Nuclear Power Institute of China, Chengdu 610213, China
[b] Key Laboratory for Mechanics in Fluid Solid Coupling Systems, Institute of Mechanics, Chinese Academy of Sciences, Beijing 100190, China

ARTICLE INFO

Keywords:
Flow-induced vibration
Fatigue damage
Two-phase flow
Tube bundles
Clearance restriction

ABSTRACT

Flow-induced vibration of the tube bundles in two-phase flow involves complicated interactions between the fluids and structures. Although a substantial number of studies have been devoted to investigating the flow-induced vibration and fluidelastic instability of the tube bundles subjected to two-phase cross-flow, the fatigue damage features of the tubes are not fully understood. In this paper, considering the effects of the turbulence random forces and the fluidelastic forces, a mathematical model of the tube bundles subjected to two-phase flow and the clearance restriction was developed. The vibration responses of the tube bundles within five void fraction conditions were calculated. The flow-induced vibration fatigue damages of the tubes were estimated based on *S-N* curves. The effects of the clearance restriction, the flow pitch velocity, and the void fraction of the two-phase flow on the fatigue damage were discussed. The numerical results demonstrate that the void fraction and flow pitch velocity of the two-phase flow have a significant influence on the fatigue damage of the tube bundles. And, the clearance restriction can change the location of the maximum fatigue damage.

1. Introduction

The flow-induced vibration fatigue damage of a steam generator has been an industry-wide concern since the 1970 s, which can become a significant mechanism impacting the reliability of the steam generator. Turbulence forces induced by the two-phase flow and the fluidelastic forces are of major significance for tube fatigue. Hence, increasing attention has been paid to the prediction of the flow-induced vibration for the tube bundles subjected to two-phase flow. The main flow excitation mechanisms of the tube bundles subjected to two-phase flow are turbulence and fluidelastic instability. Several studies have been performed to investigate the two flow excitation mechanisms.

Fluidelastic instability is an important excitation mechanism that may cause a short term failure of the steam generator tubes. Since the 1980 s, to predict the critical velocity of the fluidelastic instability of the tube bundles subjected to cross-flow, several fluidelastic force models were proposed by the scholars. Tanaka and Takahara [1] proposed the unsteady fluid force model which can be regarded as three kinds of forces: the inertia force due to the added mass of the fluid; the damping force due to the fluid; the stiffness force due to the dynamic pressure and cylinder displacement. This unsteady fluid force model can be utilized to predict the critical velocity of the fluidelastic instability of the tube bundles in cross-flow. The major drawback of the unsteady fluid force model is that all the relevant fluid force coefficients must be measured for each tube array pattern. Lever and Weaver [2] developed a simple first principle model to

* Corresponding author.
E-mail address: laijiang1983@163.com (J. Lai).

https://doi.org/10.1016/j.ymssp.2021.108442
Received 3 January 2021; Received in revised form 24 August 2021; Accepted 10 September 2021
Available online 23 September 2021

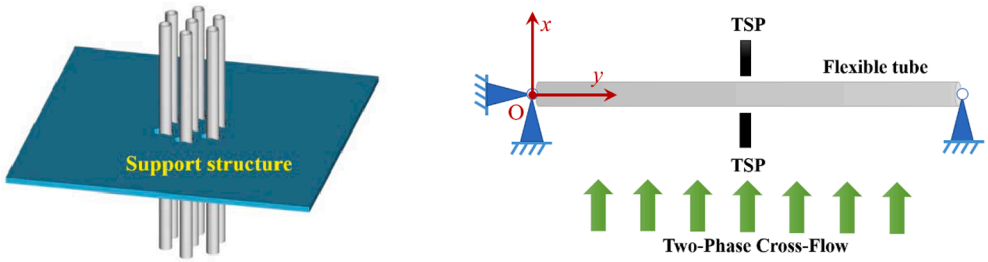

Fig. 1. Schematic diagram of tube bundles subjected to two-phase cross-flow and clearance restriction.

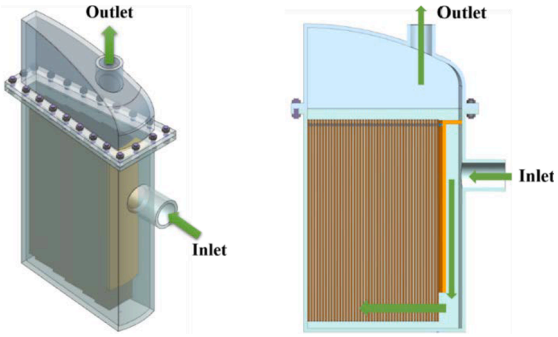

Fig. 2. Schematic diagram of the experimental model.

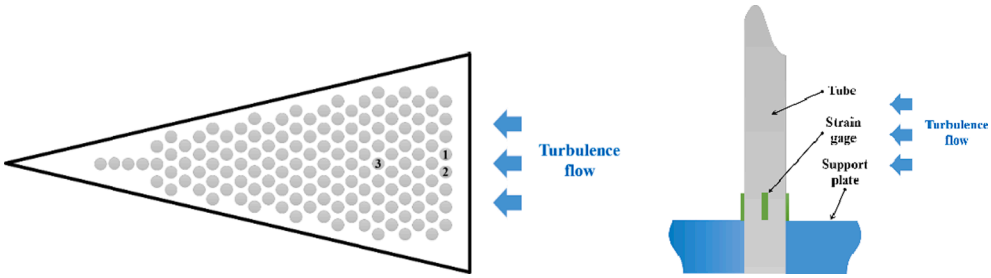

Fig. 3. Schematic diagram of the measured tubes.

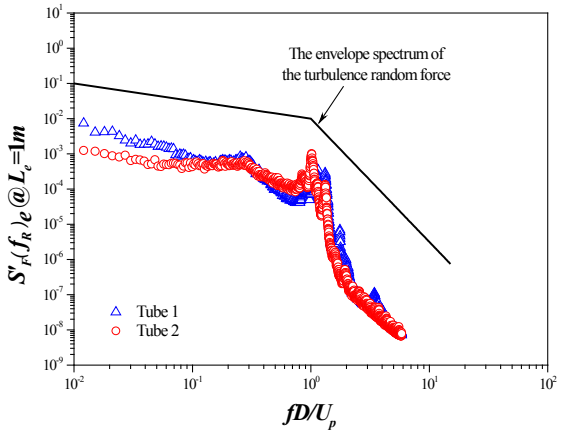

Fig. 4. The envelope spectrum of the turbulence random force.

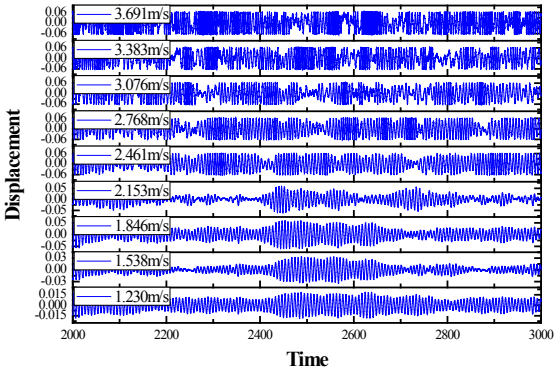

Fig. 5. Dynamic responses of the tube for 0% void fraction.

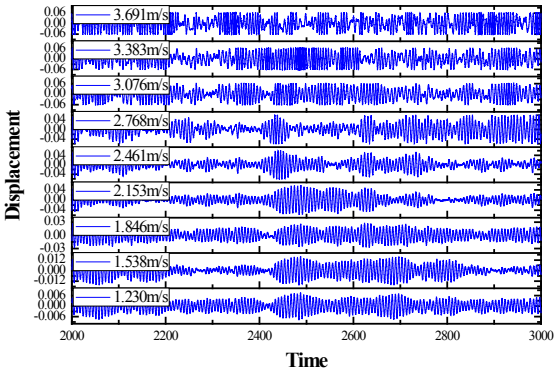

Fig. 6. Dynamic responses of the tube for 20% void fraction.

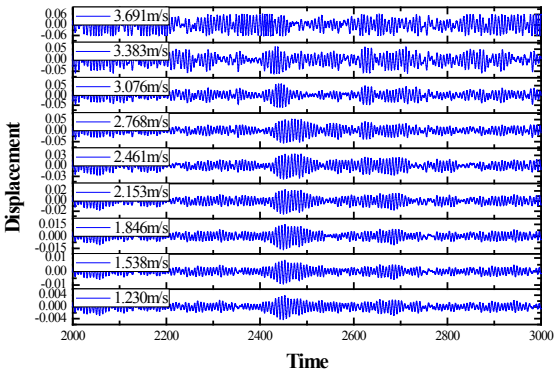

Fig. 7. Dynamic responses of the tube for 40% void fraction.

predict the threshold of the fluidelastic instability of a full tube array in cross-flow, requiring no measured fluid force coefficients. Paidoussis et al. [3] developed a full linear unsteady potential-flow solution for fluid flowing across the tube bundles which is consistent with certain basic physical checks. An improved quasi-static fluid force model was developed by Price and Paidoussis [4] to investigate the fluidelastic instability of cylinder rows subjected to cross-flow. For the high mass-damping parameters, the fluidelastic instability of the tube bundles is controlled by the stiffness mechanism. Paidoussis et al. [5] presented a semianalytical model to predict the threshold of the fluidelastic instability controlled by fluid-dynamic stiffness terms.

Turbulence is another important excitation mechanism that may cause the fatigue and fretting wear of the steam generator tubes. Taylor et al. [6] performed two experiments to determine the characteristics of the random excitation forces acting on the tube bundles in two-phase cross-flow. Their experimental results indicated that the flow rate and the void fraction have a great effect on the excitation forces. Based on the available experimental data, Langre and Villard [7] proposed an upper bound on the magnitude of the random buffeting excitation forces that apply to tube bundles in two-phase cross-flow. They found that the dynamic pressure, viscosity,

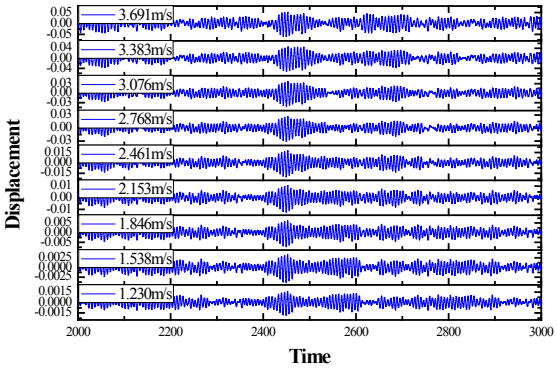

Fig. 8. Dynamic responses of the tube for 60% void fraction.

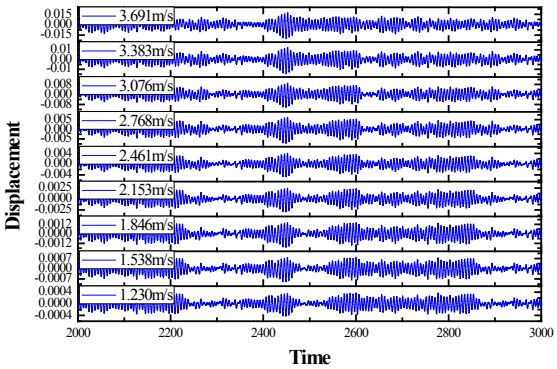

Fig. 9. Dynamic responses of the tube for 80% void fraction.

or surface tension were not relevant to the dimensionless spectra of the random fluid forces. Taylor and Pettigrew [8] carried out several experiments to measure the random fluid forces that apply to tubes in two-phase cross-flow. The data from these experiments were utilized to determine the suitable guidelines for random excitation forces. Zhang et al. [9] measured the vibration excitation force acting on a rotated triangular tube array subjected to two-phase cross-flow. Some unexpected quasi-periodic forces were observed in the experiments. Xu et al. [1011] used an inverse analysis method based on the oscillation displacements to investigate the hydrodynamic force acting on the cylinders.

Along with the development of the computer industry, numerical calculation is widely used in the computation hydrodynamics. Pedro et al. [12] used a computational fluid mechanics (CFD) methodology involving the tube motion and dynamic re-meshing to simulate the unsteady flow in a normal triangular tube array. Parrondo et al. [13] calculated the fluctuating flow in a parallel triangular tube array with the pitch-to-diameter ratio of 1.57. The simulations were developed with a commercial code to solve the 2D-URANS equations. Lai et al. established the CFD models to determine the slip ratio between the water phase and the air phase [14], and the periodic fluid force in a rotated triangular tube array [15], respectively. The correctness of the CFD calculation was verified by the experimental results.

Based on these proposed fluid force model, the fluidelastic instability and the nonlinear dynamics of the tube bundles subjected to two-phase flow were investigated. Rottmann and Popp [16] used a simple "tube-in-channel-flow" model to investigate the fluidelastic instability of a parallel triangular tube bundle. Feenstra et al. [17] conducted several experiments to measure the flow-induced vibration responses and the threshold of the fluidelastic instability of the tube bundles in a cross-flow of refrigerant 11. They found that the vortex shedding could be disrupted by a small amount of bubbles in the flow. An experimental study was carried out by Chung and Chu [18] to investigate the fluidelastic instability of the normal square tube array and the rotated square tube array with the same pitch-to-diameter ratio of 1.633 in air–water two-phase cross-flow. The experimental results indicated that the vibration characteristics of the rotated square tube array are quite different from those of the normal square tube array in the two-phase flow. Mahon and Meskell [19] investigated the interaction between the acoustic resonance and the fluidelastic instability in a normal triangular tube array. They found that the time delay between the flow field and the tube motion may be modified by the acoustic resonance. Zhao et al. [20] investigated the dynamics of the tube bundles subjected to cross-flow. The vibration characteristics of two tubes with in-line and parallel configurations were discussed. Palomar and Meskell [21] used a theoretical-CFD hybrid methodology to investigate the fluidelastic instability of a normal triangular tube array subjected to cross-flow. The numerical results illustrated that the Reynolds number has a great effect on the threshold of the fluidelastic instability. In our previous studies, a series of experimental and theoretical studies have been carried out to investigate the fluidelastic instability of a rotated triangular tube array subjected to two-phase flow [22–25], and the mathematical models were presented to study the nonlinear dynamics of the tube bundles subjected to two-phase flow and loose support [26–28].

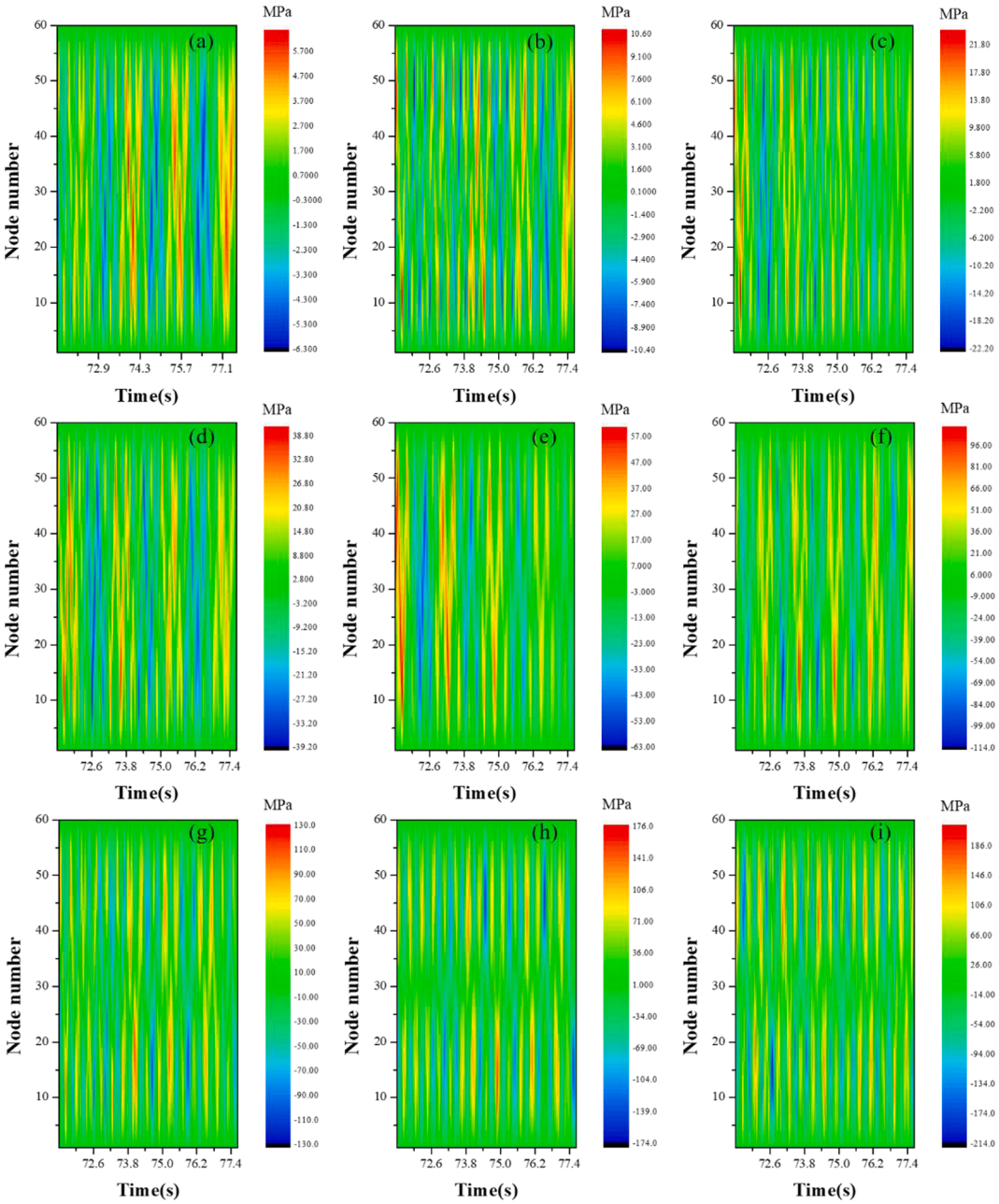

Fig. 10. Contour of the stress variations of the tube for 0% void fraction: (a) 1.230 m/s; (b) 1.538 m/s; (c) 1.846 m/s; (d) 2.153 m/s; (e) 2.461 m/s; (f) 2.768 m/s; (g) 3.076 m/s; (h) 3.383 m/s; (i) 3/691 m/s.

It is known that the fatigue breakage is one important damage style induced by the flow-induced vibration. Forecasting the tube bundles' fatigue life is very important to the security of a steam generator. As mentioned above, despite a lot of theoretical and experimental studies have been performed to analyze the flow-induced vibration and the fluidelastic instability of the tube bundles in cross-flow, few have considered the influence of the flow-induced vibration on the fatigue damage of the tube bundles. Especially, the tubes of a steam generator are always constrained by the support structures. In general, there is a gap between the tubes and the support structures which may lead to a collision. The interacton forces between the tube bundles and the support structures may affect the fatigue life of the tubes. Therefore, it is still a problem deserving further investigations for the flow-induced vibration fatigue damage of the tube bundles subjected to two-phase flow and the clearance restriction.

In this study, considering the effect of the fluidelastic force and the turbulence random force, a mathematical model of the tube bundles subjected to two-phase cross-flow and the clearance restriction was developed. Based on S-N curves by using the numerical results of the vibration responses, the flow-induced vibration fatigue damages of the tube bundles within different void fraction

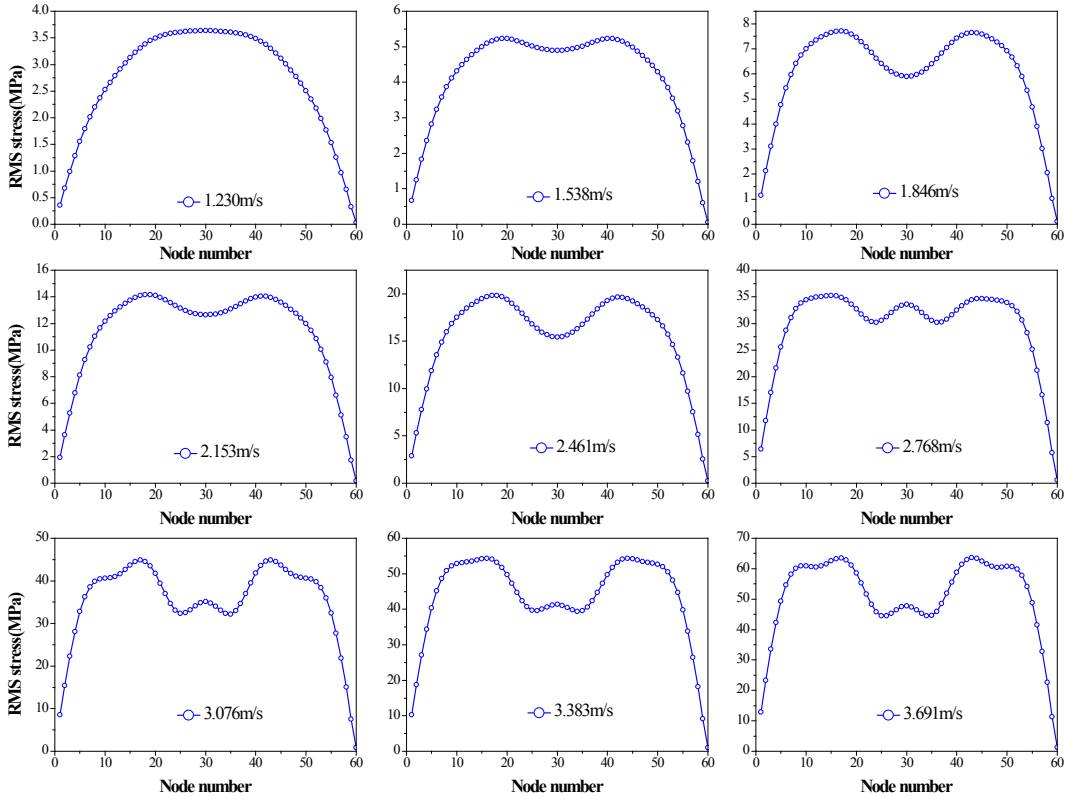

Fig. 11. RMS stress of the tube for 0% void fraction.

conditions were estimated. More importantly, the effects of the clearance restriction, the flow pitch velocity, and the void fraction of the two-phase flow on the fatigue damage were discussed.

A detailed implementation procedure for the fatigue evalutaion methodology is as follows:

① To determine the equivalent power spectral density (EPSD) of the turbulent excitation force acting on the tube bundles by experimental measurement.

② To calculate the vibration responses of the tube bundles system with clearance restriction subjected to fluidelastic force and turbulent force. The fluidelastic force is produced by a coupling between the tube motion and the flowing fluid. The turbulent force is transformed from the EPSD curve into a force–time record.

③ To evaluate the fatigue damage of the tube bundles system based on the S-N approach. As the flow-induced stress cycles are random, the Rainflow Cycle Counting method is used to calculate the distribution of stress amplitudes.

2. Two-phase flow-induced vibration analysis

2.1. Theoretical analysis

In a steam generator, the tube bundles are threaded through the support structures such as the tube support plate (TSP) and the anti-vibration bars (ATVs). Typically, to avoid the effect of the thermal expansion or contraction, there would be a small gap between the tube bundles and the support structures, as shown in Fig. 1. Therefore, when the vibration amplitude of the tube is larger than the gap, a collision occurs. In the present study, we treated the flexible tube as a simply-supported tube with a clearance restriction at the middle of the span. Considering the effects of the fluidelastic force and the turbulence random force, the motion equation of a flexible tube in a tube array subjected to two-phase cross-flow and clearance restriction can be written as:

$$EI\frac{\partial^4 w}{\partial y^4}+c_t\frac{\partial w}{\partial t}+m_t\frac{\partial^2 w}{\partial t^2}+\delta(y-y_a)f(w)=F_{FEI}(\ddot{w},\dot{w},w)+F_{turbulence}(t) \tag{11}$$

Then, introducing the following the non-dimensional quantities:

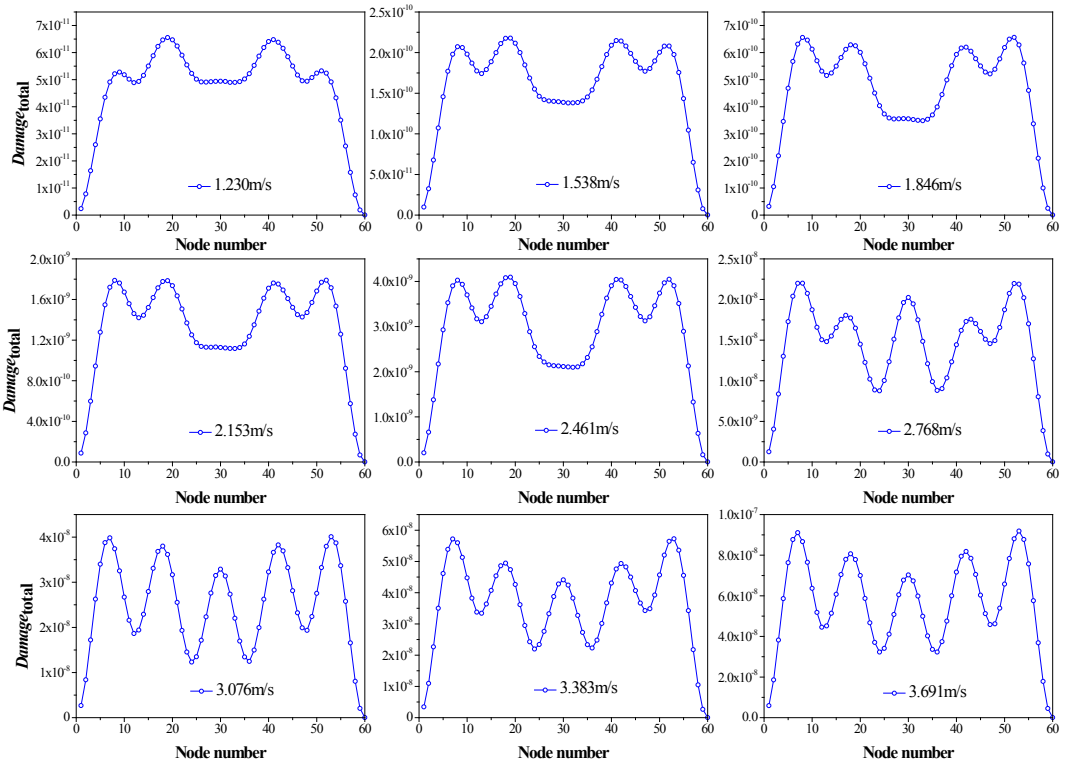

Fig. 12. Spanwise distributions of fatigue damage for 0% void fraction.

$$\eta = \frac{w}{D}, \quad \xi = \frac{y}{L}, \quad \tau = \lambda_1^2\sqrt{\frac{EI}{m_t L^4}}t = \Omega t, \quad \varsigma = \frac{c_t}{\Omega m_t}, \quad m^* = \frac{m_t}{\rho D^2}, \quad U^* = \frac{2\pi U_\infty}{D\Omega},$$
$$\alpha = \frac{1}{1 + 4m^*/(\pi C_{ma})}, \quad \omega^* = \frac{\omega}{\Omega} \tag{12}$$

where L is the tube length, λ_1 is the dimensionless eigenvalue of the first-order mode for a simply supported beam, C_{ma} is the added mass coefficient which can be expressed as:

$$C_{ma} = \frac{(D_e/D)^2 + 1}{(D_e/D)^2 - 1} \tag{13}$$

the partial differential equation of the motion of the tube bundles considering the effects of two-phase cross-flow and clearance restriction can be rewritten as:

$$\frac{1}{1-\alpha}\frac{\partial^2\eta}{\partial\tau^2}(\xi,\tau) + \left[\varsigma - \frac{U^{*2}C_F sin\Phi_F}{8\pi^2 m^* \omega^*}\right]\frac{\partial\eta}{\partial\tau}(\xi,\tau) + \frac{1}{\lambda_1^4}\frac{\partial^4\eta}{\partial\xi^4}(\xi,\tau)$$
$$-\left[\frac{U^{*2}C_F cos\Phi_F}{8\pi^2 m^*} - \frac{\alpha\omega^{*2}}{1-\alpha}\right]\eta(\xi,\tau) + \delta(\xi-\xi_b)f^*(\eta) = F(\tau) \tag{14}$$

where $F(\tau)$ is the time history of the dimensionless random excitation force, which can be expressed as:

$$F(\tau) = \sum_{j=1}^{N} a_j cos\left(\omega_j\tau + \theta_j\right) \tag{15}$$

where θ_j is the random variable from $0 \sim 2\pi$ which are completely independent of each other, a_j is the gaussian random variable, which can be obtained by:

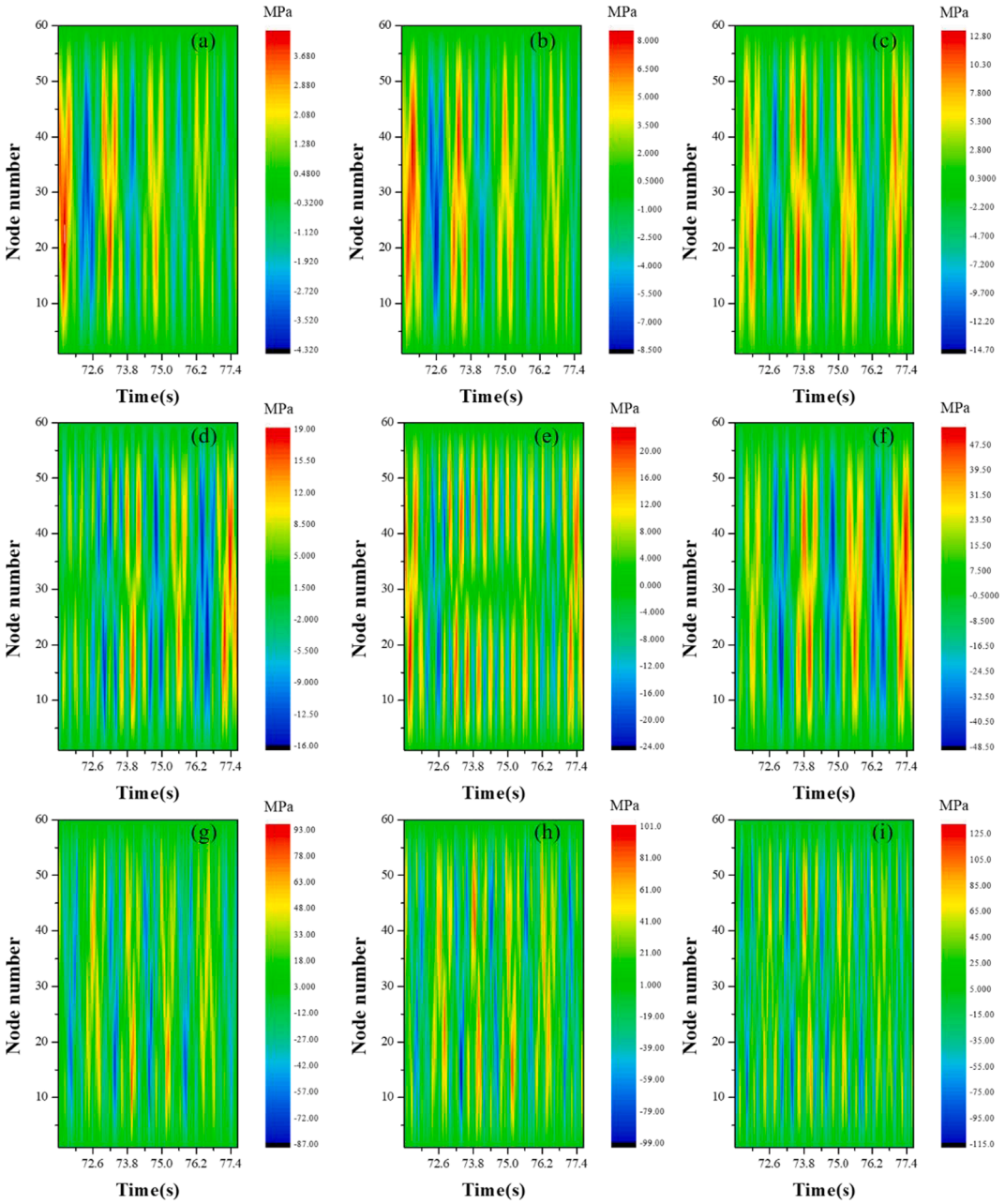

Fig. 13. Contour of the stress variations of the tube for 20% void fraction: (a) 1.230 m/s; (b) 1.538 m/s; (c) 1.846 m/s; (d) 2.153 m/s; (e) 2.461 m/s; (f) 2.768 m/s; (g) 3.076 m/s; (h) 3.383 m/s; (i) 3/691 m/s.

$$\begin{aligned} a_j^2 &= 4S_F(\omega_j)\Delta\omega \\ \Delta\omega &= \frac{\omega_u - \omega_1}{N} \\ \omega_j &= \omega_1 + \left(j - \frac{1}{2}\right)\Delta\omega \end{aligned} \tag{16}$$

where ω_u is the upper limit value of the frequency, ω_1 is the lower limit value of the frequency.

Based on equation (15) and (16), one of the time domain solutions of the equivalent power spectral density, $F(\tau)$, can be calculated. Thus, once the flow pitch velocity of the two-phase flow is determined, the time series of the turbulence excitation acting on the tube can be obtained.

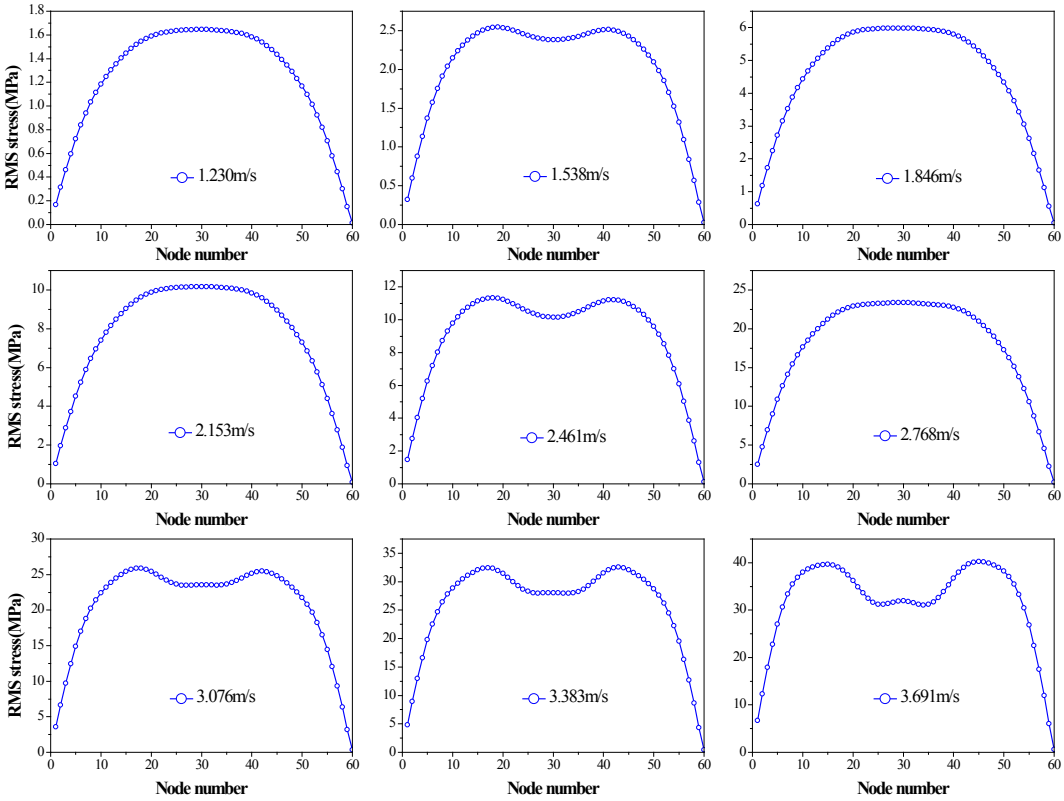

Fig. 14. RMS stress of the tube for 20% void fraction.

According to the Galerkin method, the solution of equation (14) can be supposed as:

$$\eta(\xi,\tau)=\sum_{i=1}^{N}\phi_i(\xi)q_i(\tau) \tag{17}$$

where $\phi_i(\xi)$ is the modal shape of the tube. In this study, the first five order modes were chosen ($N=5$).

Using the Galerkin expansion and modal truncation techniques, a set of ordinary differential equations can be deduced from the partial differential equation, as follows:

$$\frac{\ddot{q}_i}{1-\alpha}+\left(\zeta-\frac{U^{*2}C_F sin\Phi_F}{8\pi^2 m^* \omega^*}\right)\dot{q}_i+\left(\frac{\lambda_i^4}{\lambda_1^4}-\frac{U^{*2}C_F cos\Phi_F}{8\pi^2 m^*}+\frac{\alpha\omega^{*2}}{1-\alpha}\right)q_i+f^*(\eta_a)\varphi_i(\xi_a)=F(\tau)$$

$$(i=1,\quad 2,\quad 3,\quad 4,\quad 5) \tag{18}$$

where η_a is the displacement at $\xi=\xi_a$.

Notice that the coupling term is the impact force between the tube and tube support plate $f^*(\eta_a)$ due to the constraint at the clearance restriction. In this study, the mathematical model presented by Paidoussis et al. [30] was used to represent properly the restraining force of clearance restriction, which can be written as:

$$f^*(\eta_a)=\kappa\left[\eta_a-\frac{1}{2}(|\eta_a+d|-|\eta_a-d|)\right]^3 \tag{19}$$

where d is the non-dimensional gap between the tubes and the support structures, κ is the non-dimensional stiffness of the clearance restriction. In this paper, κ is chosen to be 5.6×10^6 in accordance with reference [31].

Notice that it is difficult to obtain the equivalent power spectral density, $\hat{S}_F(f_R)_e$, in tube bundles. Therefore, according to the analysis above, an experiment was carried out to measure the power spectral density of the excitation force in the next section. Then, according to equation (15) and equation (16), the force time history can be obtained.

2.2. Experimental analysis

This section gives a brief introduction of our previous experiment to obtain the turbulence random forces acting on the tube bundles

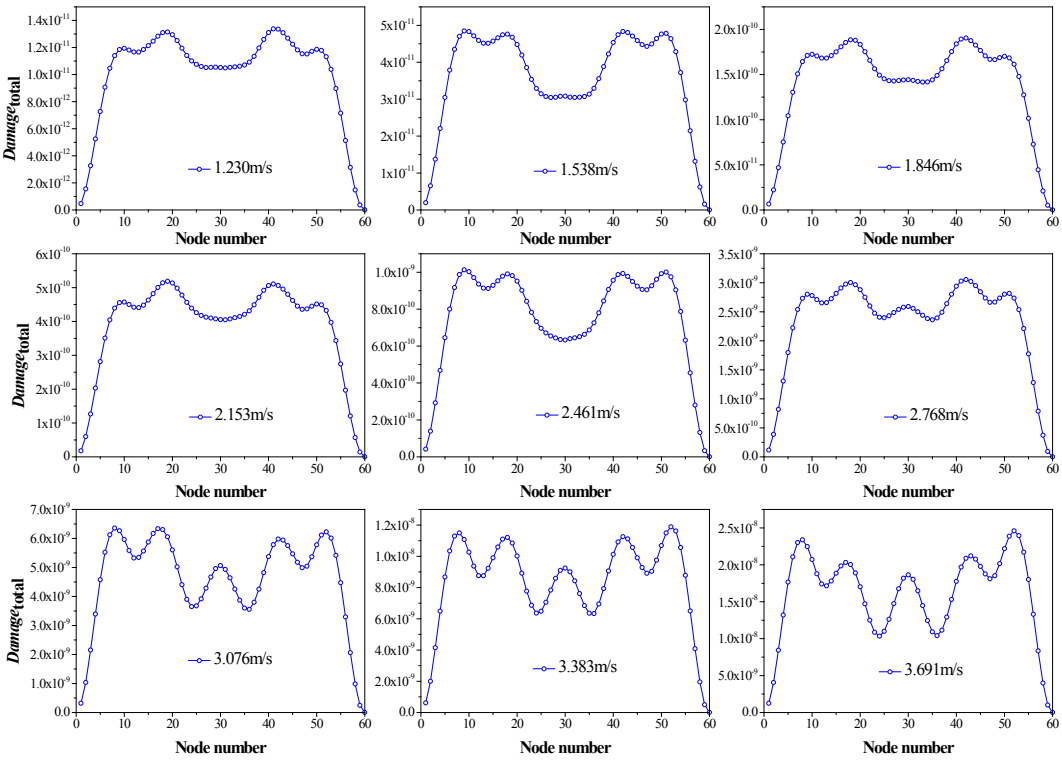

Fig. 15. Spanwise distributions of fatigue damage for 20% void fraction.

which will be used to calculate the vibration responses of the tube bundles in the next section. The experimental model was designed by arranging a rotated triangular tube array into a fan shape, as shown in Fig. 2. All the tube bundles were fixed with tube support plates. The span lengths of the tube bundles used in this experiment are typical of span lengths in steam generators. The tube diameter D is 0.01745 m, the pitch-to-diameter ratio is 1.48. As shown in Fig. 3, the strain gauges were mounted on three tubes near the tube support plate to measure the tube bundles vibration responses. Experiments were performed for five flow pitch velocity conditions. All measurements were conducted at room temperature (approximately 20 °C).

According to equation (10), the equivalent power spectral density of the turbulence random force acting on the tube bundles can be obtained. The envelope spectrum of the turbulence random force can be written as:

$$\widehat{S}_F(f_R) = \begin{cases} 10^{-2}(f_R)^{-0.5}, & 0.01 < f_R \leqslant 1 \\ 10^{-2}(f_R)^{-3.5}, & 1 < f_R \end{cases} \tag{20}$$

The envelope spectrum of the turbulent excitation force was shown in Fig. 4.

By substituting the envelope spectrum of the turbulent excitation force into equation (15) and (16), the time series of the turbulent force, $F(\tau)$, acting on the tube at a certain flow pitch velocity condition can be determined.

2.3. Vibration response calculation

The finite difference solution was adopted to divide the flexible tube into 59 elements with 60 nodes. Then, based on the theoretical and experimental studies in the last two sections, the vibration responses of the tube bundles considering the effects of the fluidelastic force and turbulence random force within the five void fraction conditions (β = 0%, 20%, 40%, 60%, and 80% void fraction, respectively) were calculated by using a fourth-order Runge-Kutta integration algorithm, with a step size of 0.01. To investigate the effects of the flow pitch velocity on the flow-induced vibration and fatigue damage of the tube bundles, nine flow pitch velocity cases were chosen in this study, which is 1.230 m/s, 1.538 m/s, 1.846 m/s, 2.153 m/s, 2.461 m/s, 2.768 m/s, 3.076 m/s, 3.383 m/s, and 3.691 m/s, respectively. As shown in Fig. 1, the support structure is at the middle of the span. When the tube vibration amplitude is larger than the gap between the tube and support structure, the collision occurs. To illustrate the impact behaviors, the vibration responses of the flexible tube with a clearance restriction at the 30th node within five void fraction conditions for the nine flow pitch velocity cases were illustrated in Fig. 5-Fig. 9, respectively. The random vibration responses of the tube can be observed in Fig. 5-Fig. 9 for all the cases considered in this study. It should be noted that the vibration amplitude of the tube increases monotonically with the increasing of the flow pitch velocity within the five void fractions. On the other hand, the vibration amplitude of the tube decreases monotonically with the increasing of the void fraction for the same flow pitch velocity condition. It is important to note that the

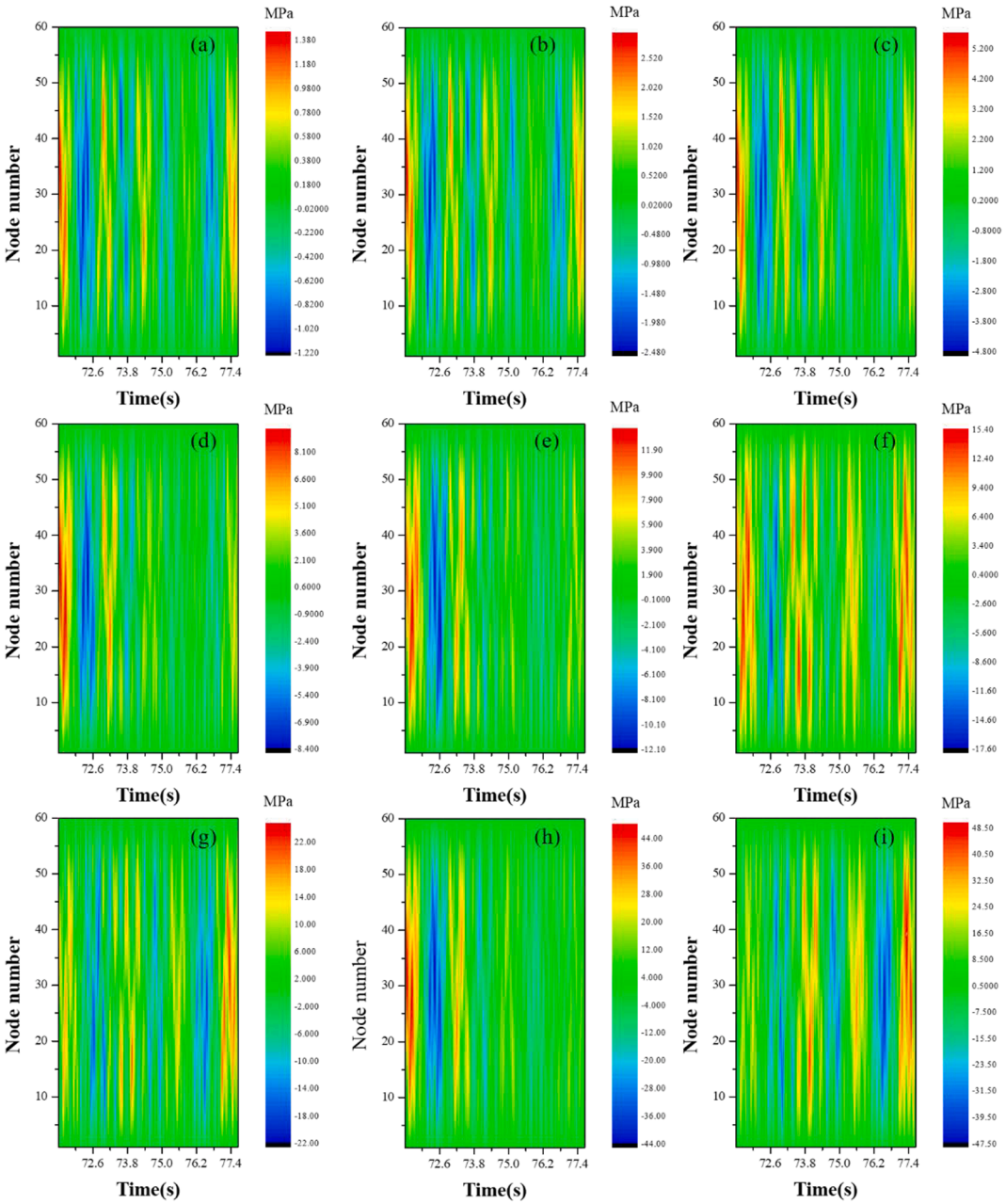

Fig. 16. Contour of the stress variations of the tube for 40% void fraction: (a) 1.230 m/s; (b) 1.538 m/s; (c) 1.846 m/s; (d) 2.153 m/s; (e) 2.461 m/s; (f) 2.768 m/s; (g) 3.076 m/s; (h) 3.383 m/s; (i) 3/691 m/s.

collision between the tube bundles and TSP may occur within the lower void fraction conditions. For 0% void fraction, when the flow pitch velocity is lower than 1.846 m/s, no collision between the tube bundles and TSP occurs. Once the flow pitch velocity is larger than 1.846 m/s, the collision can be observed clearly in Fig. 5. For the 20% void fraction, when the flow pitch velocity is lower than 2.461 m/s, no collision between the tube bundles and TSP occurs. Once the flow pitch velocity is larger than 2.461 m/s, the collision can be observed in Fig. 6. For the 40% void fraction, when the flow pitch velocity is lower than 3.076 m/s, no collision between the tube bundles and TSP occurs. Once the flow pitch velocity is larger than 3.076 m/s, the collision can be observed in Fig. 7. The results show that with the increase of the flow pitch velocity, the collision frequency increases. As shown in Figs. 8 and 9, at the 60% and 80% void fraction conditions, no collision has been observed for the range of the flow pitch velocity considered in this study.

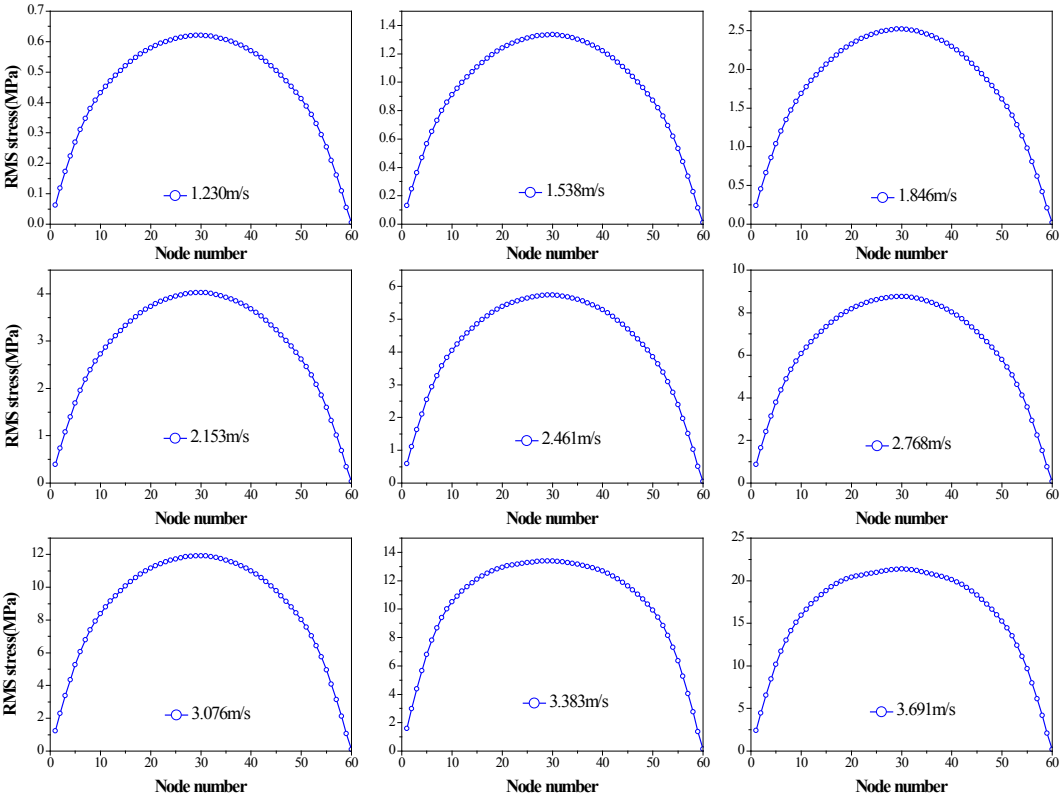

Fig. 17. RMS stress of the tube for 40% void fraction.

3. Fatigue damage analysis

3.1. Methodology for fatigue damage estimation

The *S-N* curve is one of the most extensively used method to estimate the fatigue damage of the tube bundles of a steam generator in nuclear engineering. In practical applications, the total fatigue damage can be estimated by the linear accumulation rule. Hence, in the present study, the Palmgren-Miner rule was employed to calculate the total fatigue damage [32], which can be expressed as:

$$Damage_{total} = \sum_i \frac{n_i}{N_i} \tag{21}$$

where $Damage_{total}$ is the total fatigue damage, N_i is the permissible number of cycles, n_i is the actual number of cycles. The relation between N_i and σ_i is defined by the *S-N* equation proposed by Tan [33], as follows:

$$lnN_i = 6.525 - 2.008ln\left(\frac{\sigma_i}{E} - 0.116\right) \tag{22}$$

The rain flow counting method was used to determine the strain cycles and corresponding ranges in fatigue damage events. The vibration displacement is expressed by equation (17), where the modal shape of a simply-supported beam can be written as:

$$\phi_i(\xi) = sin\frac{i\pi}{L}\xi \tag{23}$$

Due to the necessity of strain signals in fatigue damage estimation, based on the theoretical of mechanics of materials, the strain signals $\varepsilon(\xi, \tau)$ at the surface of the tube can be written as:

$$\varepsilon(\xi,\tau) = \frac{D}{2}\frac{\partial^2\eta(\xi,\tau)}{\partial\xi^2} \tag{24}$$

$$\varepsilon(\xi,\tau) = -\frac{D}{2}\left(\frac{i\pi}{L}\right)^2 \sum_{i=1}^{\infty} q_i(\tau) sin\frac{i\pi\xi}{L} \tag{25}$$

The only unknown parameter $q_i(\tau)$ has been calculated in the last section. Hence, the stress signals $\sigma(\xi, \tau)$ can be easily obtained

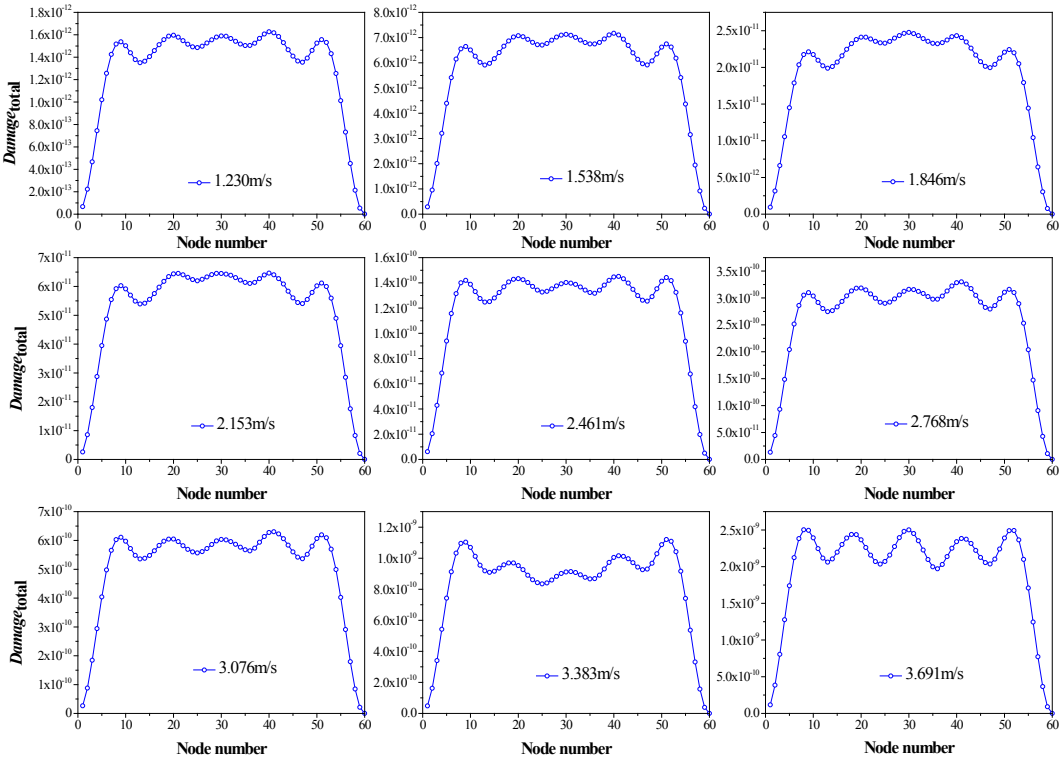

Fig. 18. Spanwise distributions of fatigue damage for 40% void fraction.

from the following equation:

$$\sigma(\xi,\tau) = E\varepsilon(\xi,\tau) = -\frac{ED}{2}\left(\frac{i\pi}{L}\right)^2 \sum_{i=1}^{\infty} q_i(\tau) sin\frac{i\pi\xi}{L} \tag{26}$$

Based on the *S-N* curve and rain flow counting method, the total fatigue damage is calculated.

3.2. Fatigue damage calculation

Fig. 10 shows the contours of spatiotemporal stress variations for the nine flow pitch velocity cases within the 0% void fraction. Fig. 11 shows the root-mean-square (RMS) stress of the flexible tube for the nine flow pitch velocity cases within the 0% void fraction. As analyzed above, when the flow pitch velocity is less than 1.846 m/s, no collision between the tube bundles and the support structure occurs, the stress is relatively well-distributed. And the maximum stress of the tube increases with the increasing of the flow pitch velocity. It is important to note that when the flow pitch velocity is larger than 1.846 m/s, the clearance restriction plays an important role on the stress distribution. The maximum stress appears at both sides of the clearance restriction, and the stress distribution is symmetric about the TSP position. Fig. 12 presents the spanwise distributions of the fatigue damage of the flexible tube for the nine flow pitch velocity cases within the 0% void fraction, respectively. It is interesting to note that when the flow pitch velocity is lower than 1.846 m/s, the distributions of the fatigue damage of the flexible tube is symmetric about the TSP location, and the positions of the maximum fatigue damage of the tube are at the 20th and 40th nodes of the tube. Due to the presence of the collision between the tube bundles and the TSP, the fatigue damage at the 30th node of the tube was increased, and the positions of the maximum fatigue damage of the tube were also changed to the 7th and 53rd nodes.

Fig. 13 shows the contours of spatiotemporal stress variations for the nine flow pitch velocity cases within the 20% void fraction. Fig. 14 shows the RMS stress of the flexible tube for the nine flow pitch velocity cases within the 20% void fraction. Similarly, the maximum stress of the tube increases with the increasing of the flow pitch velocity. When the flow pitch velocity is less than 2.461 m/s, no collision between the tube bundles and the support structure occurs, the stress is relatively well-distributed. When the flow pitch velocity is larger than 2.461 m/s, the collision occurs, and the maximum stress appears at the both sides of the clearance restriction, and the stress distribution is also symmetric about the TSP position. Fig. 15 presents the spanwise distributions of the fatigue damage of the flexible tube for the nine flow pitch velocity cases within the 20% void fraction, respectively. It also can be seen that the spanwise distributions of the fatigue damage of the tube within the 20% void fraction are similar to those in the 0% void fraction, and the clearance restriction plays an important role in the distribution of the fatigue damage. It should be noted that the positions of the maximum fatigue damage are at the 20th and 40th nodes when the flow pitch velocity ranging from 1.230 m/s to 3.383 m/s which are

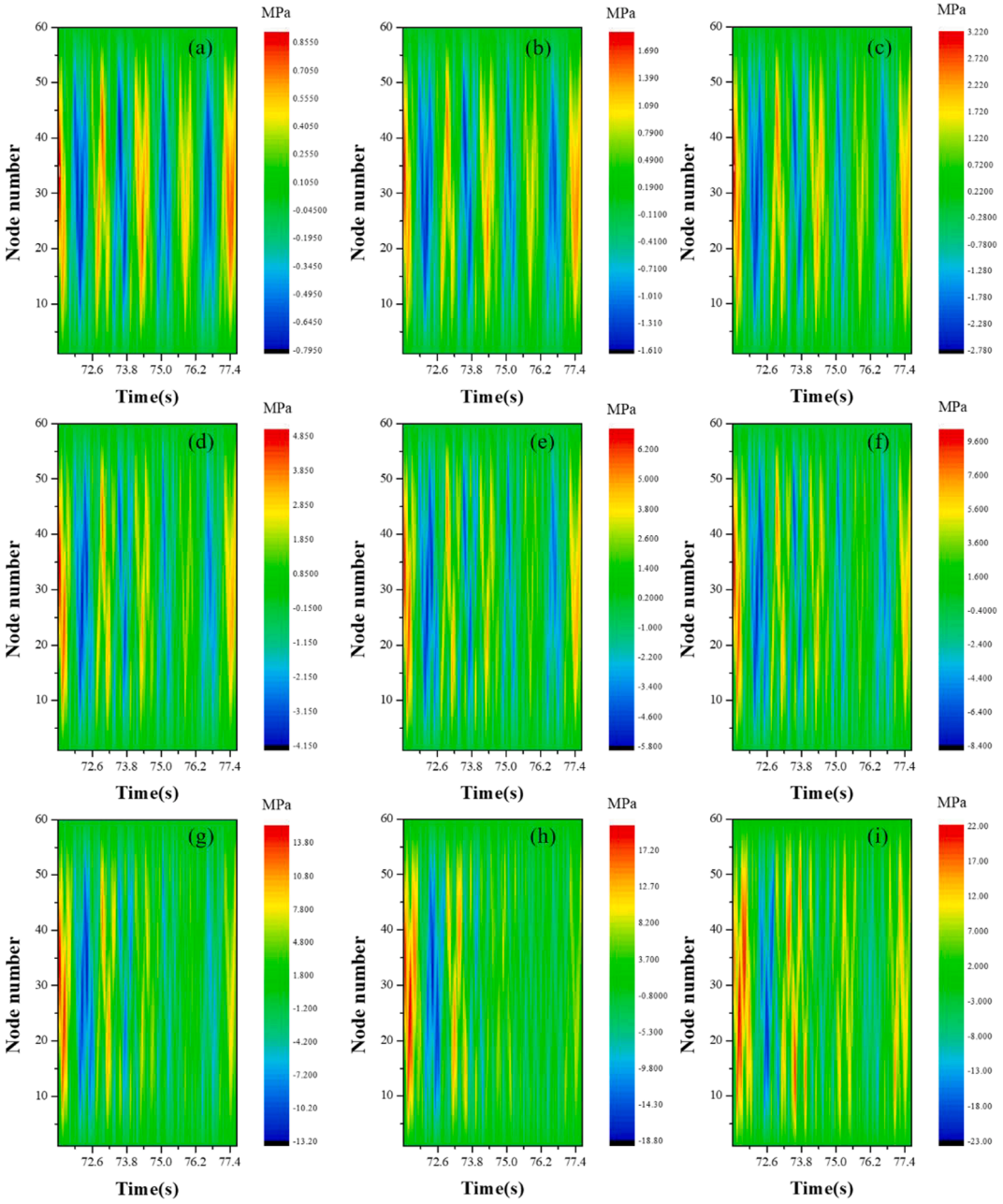

Fig. 19. Contour of the stress variations of the tube for 60% void fraction: (a) 1.230 m/s; (b) 1.538 m/s; (c) 1.846 m/s; (d) 2.153 m/s; (e) 2.461 m/s; (f) 2.768 m/s; (g) 3.076 m/s; (h) 3.383 m/s; (i) 3/691 m/s.

different from those in the 0% void fraction. At $U_p = 3.691$ m/s, the positions of the maximum fatigue damage are changed to the 7th and 53rd nodes.

Fig. 16 shows the contours of spatiotemporal stress variations for the nine flow pitch velocity cases within 40% void fraction. It can be seen that the stress of the flexible tube varies at different times. With the increase of the flow pitch velocity, the stress of the tube increases. Especially, when the collision occurs, the maximum stress of the tube increases evidently. Fig. 17 shows the RMS stress of the flexible tube for the nine flow pitch velocity cases within the 40% void fraction. The maximum stress is at the location of the 30th node for all the nine flow pitch velocity cases, indicating that the influence of the collision between the tube and the support structure on the stress distribution of the tube was slight within the 40% void fraction for the flow pitch velocity range considered in the present study. Fig. 18 presents the spanwise distributions of the fatigue damage of the flexible tube for the nine flow pitch velocity cases within the 40% void fraction, respectively. The fatigue damage of the tube increases with the increasing of the flow pitch velocity. Due to the less effect of the collision between the tube bundles and the support structure, the uniformity of the spanwise distributions of fatigue

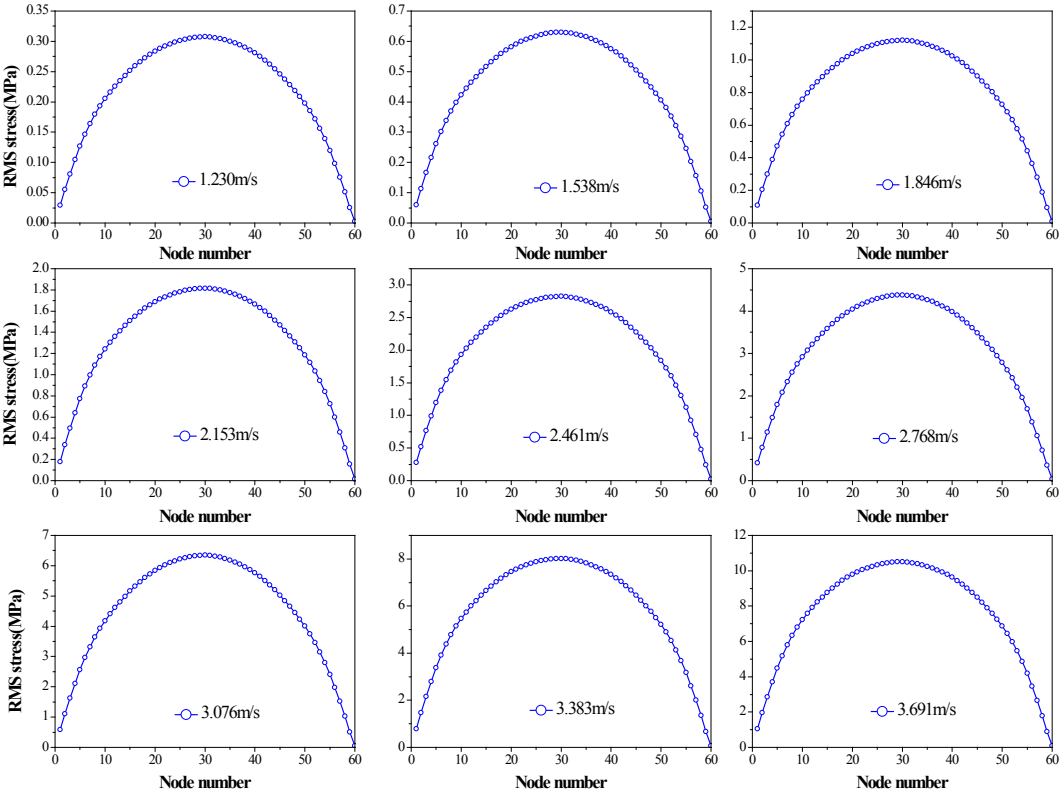

Fig. 20. RMS stress of the tube for 60% void fraction.

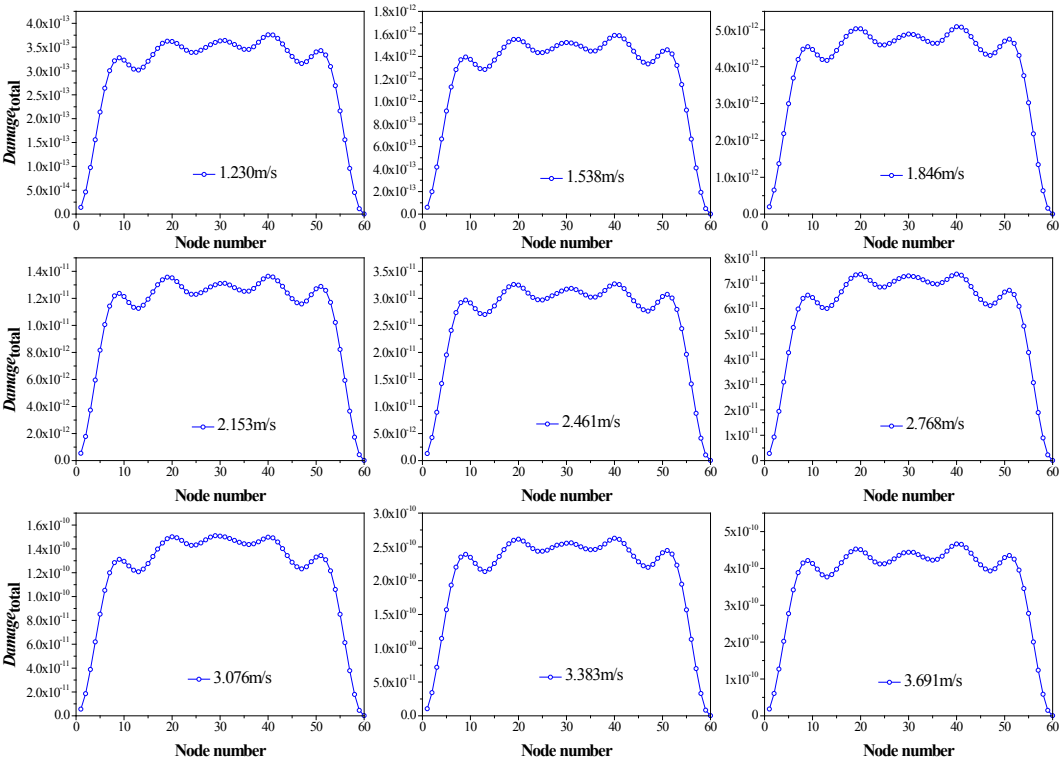

Fig. 21. Spanwise distributions of fatigue damage for 60% void fraction.

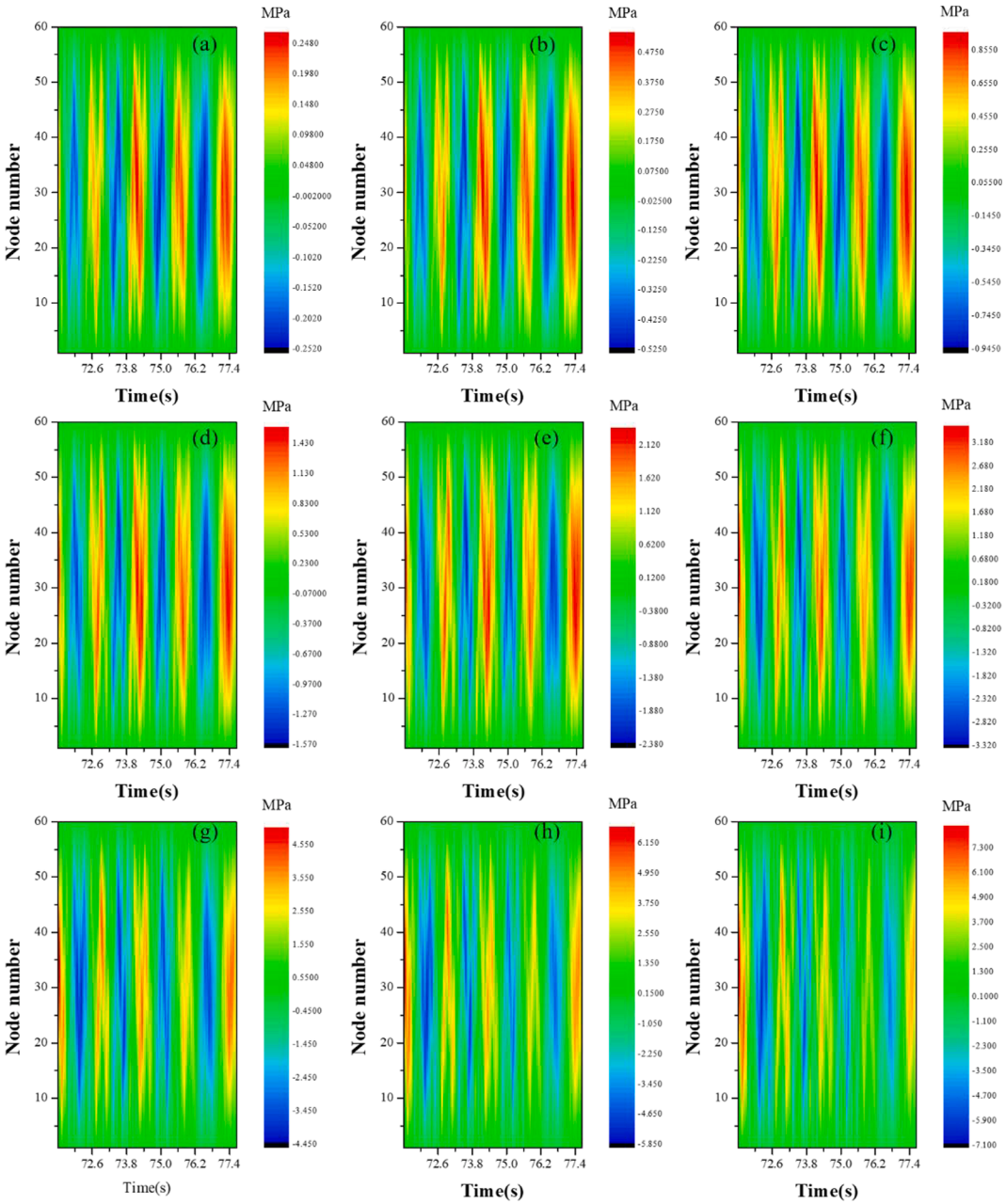

Fig. 22. Contour of the stress variations of the tube for 80% void fraction: (a) 1.230 m/s; (b) 1.538 m/s; (c) 1.846 m/s; (d) 2.153 m/s; (e) 2.461 m/s; (f) 2.768 m/s; (g) 3.076 m/s; (h) 3.383 m/s; (i) 3/691 m/s.

damage can be observed.

Fig. 19 presents the contours of spatiotemporal stress variations for the nine flow pitch velocity cases within the 60% void fraction. Similarly, the stress of the tube increases with the increasing of the flow pitch velocity. It should be noted that the periodic vibration of the tube was induced by the two-phase cross-flow when the flow pitch velocity is lower than 2.461 m/s, and the periodic fluctuation of the stress can be obviously observed. When the flow pitch velocity is larger than 2.461 m/s, the turbulence-induced vibration of the tube bundles occurs, the periodic fluctuation of the stress disappears. The RMS stress of the flexible tube for the nine flow pitch velocity cases within the 60% void fraction was illustrated in Fig. 20. No collision between the tube bundles and the TSP occurs, thus the RMS stress distribution is similar to a typical simply-supported beam. As shown in Fig. 21, the spanwise distributions of the fatigue damage of the flexible tube for the nine flow pitch velocity cases within the 60% void fraction appear to be similar to each other, though the fatigue damage of the flexible tube increases with the increasing of the flow pitch velocity.

The contours of spatiotemporal stress variations, the RMS stress, and the spanwise distributions of the fatigue damage of the flexible

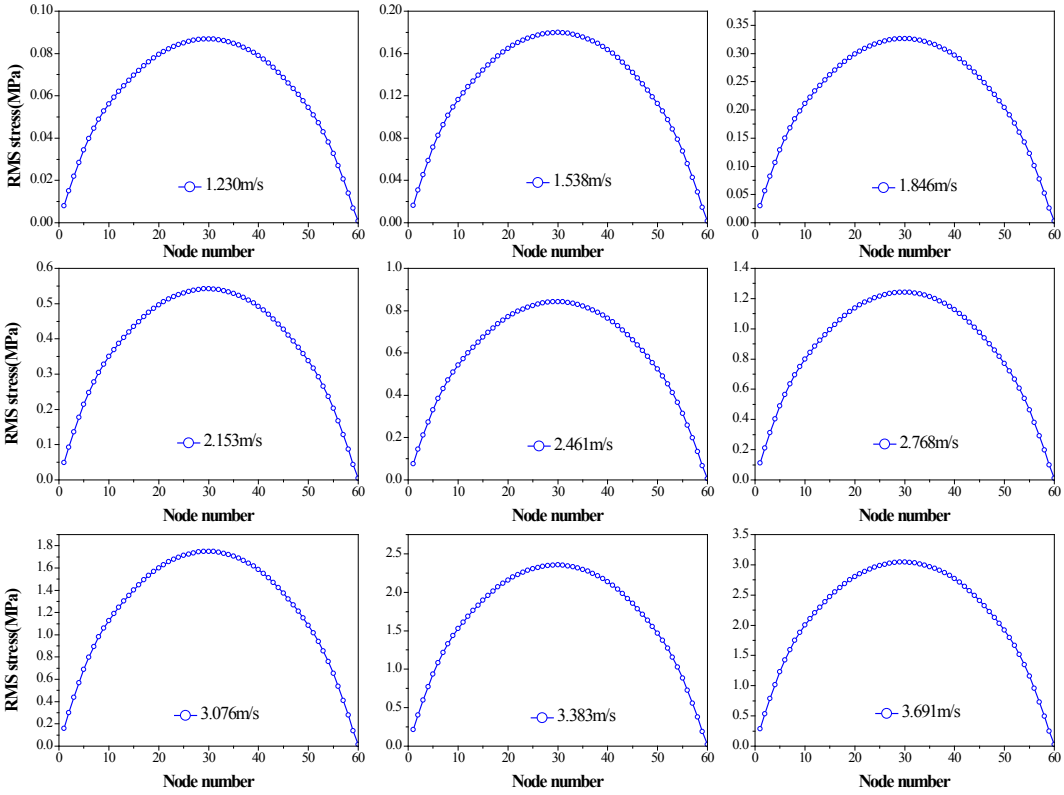

Fig. 23. RMS stress of the tube for 80% void fraction.

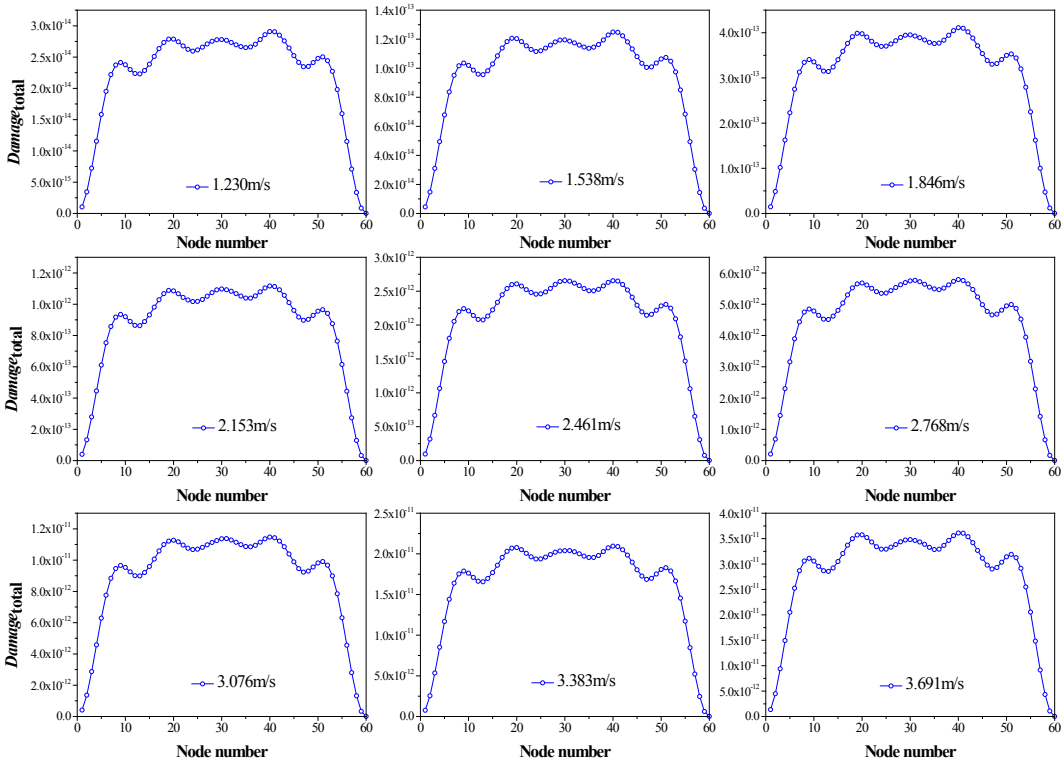

Fig. 24. Spanwise distributions of fatigue damage for 80% void fraction.

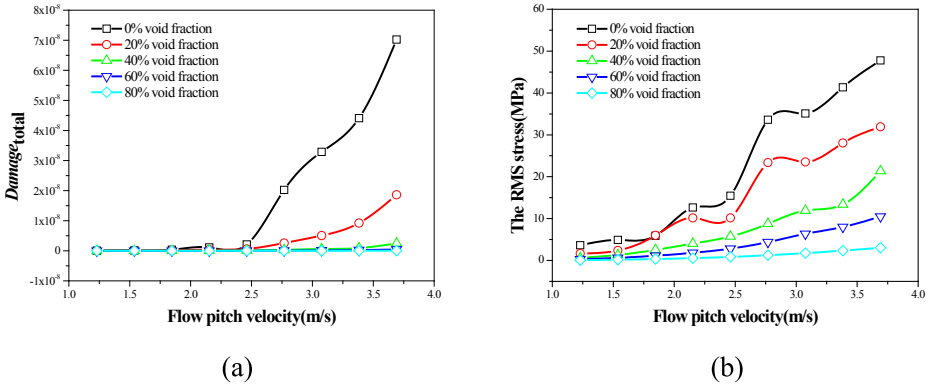

Fig. 25. (a) Variation of the fatigue damage with respect to the flow pitch velocity of the two-phase flow; (b) Variation of the RMS stress with respect to the flow pitch velocity of the two-phase flow.

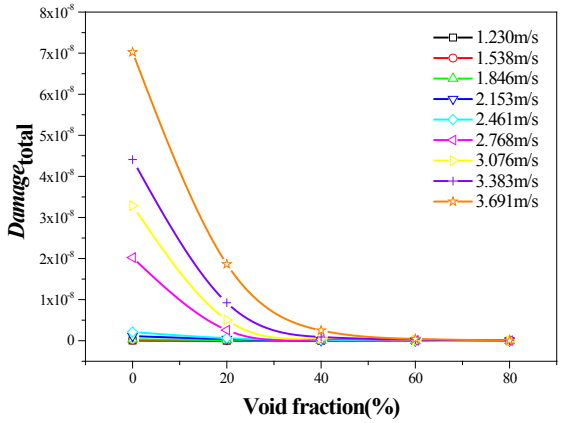

Fig. 26. Variation of the fatigue damage with respect to the void fraction of the two-phase flow.

tube for the nine flow pitch velocity cases within 80% void fraction were illustrated in Fig. 22 ~ Fig. 24, respectively. There are significant similarities of the stress distributions and the fatigue damage distribution of the tube between the two void fraction conditions (60% void fraction and the 80% void fraction).

4. Discussion

According to the numerical results obtained in the last sections, it is obvious that the void fraction and flow pitch velocity are the important parameters to the flow-induced vibration fatigue damage of the tube bundles subjected to two-phase flow and the clearance restriction. Thus, the influences of the flow pitch velocity and the void fraction of the two-phase flow on the fatigue damage were discussed quantitatively in this section.

The variation of the fatigue damage and the RMS stress of the 30th node within the five void fraction conditions ($\beta = 0\%$, 20%, 40%, 60%, and 80% void fraction, respectively) with respect to the flow pitch velocity was presented in Fig. 25. As shown in Fig. 25(a), when the flow pitch velocity is lower than 2.461 m/s, the fatigue damage of the tube bundles increases slowly with the increasing of the flow pitch velocity, and the effects of the void fraction on the fatigue damages of the three nodes are inconspicuous. But, it is interesting to note that when the flow pitch velocity is larger than 2.461 m/s, as the increase of the flow pitch velocity, the fatigue damage degree increases quickly within the lower void fractions, especially in 0% void fraction. However, for the high void fraction conditions, as the flow pitch velocity of the two-phase flow increases, the fatigue damage has a little increase. It can be seen from Fig. 25(b) that when the flow pitch velocity is larger than 2.461 m/s, due to the collision between tube bundles and the TSP, a large increase in the RMS stress occurs with a little increase in the flow pitch velocity in 0% and 20% void fractions. Similarly, when the collision occurs at $U_p = 3.383$ m/s, the RMS stress of the tube increases noticeably within 40% void fraction. The results indicate that the collision between the tube bundles and the support structures has a significant effect on the fatigue damage of the tube. In other words, the gap between the tube bundles and the clearance restriction is an important parameter to estimate the fatigue life of the tube. Once the amplitude of the flow-induced vibration is larger than the gap between the tube and the TSP, the fatigue life may be reduced significantly.

The variation of the fatigue damage of the 30th node for the nine flow pitch velocity cases ($U_p = 1.230$ m/s, 1.538 m/s, 1.846 m/s, 2.153 m/s, 2.461 m/s, 2.768 m/s, 3.076 m/s, 3.383 m/s, and 3.691 m/s, respectively) respect to the void fraction were illustrated in

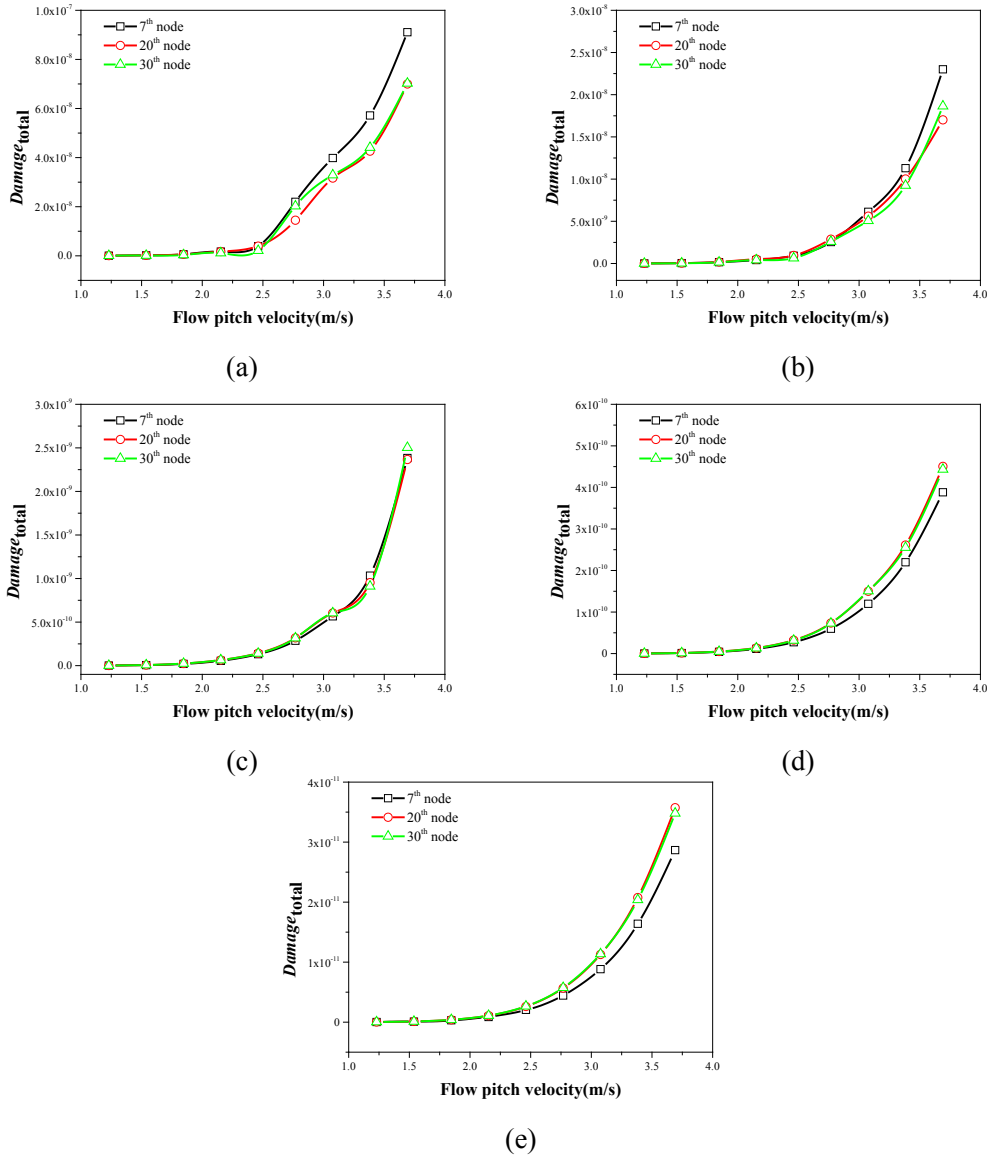

Fig. 27. Comparison of the fatigue damage between the 7th, 20th, and 30th nodes: (a) 0% void fraction; (b) 20% void fraction; (c) 40% void fraction; (d) 60% void fraction; (e) 80% void fraction.

Fig. 26. With the increase of the void fraction of the two-phase flow, the fatigue damage of the tube decreases quickly. The main reason is that in the high void fraction conditions, the natural frequencies of the tube are higher than those in the low void fraction conditions. The attenuation of the fatigue damage of the tube can be attributed to the lower-order dominant modes of the tube bundles. The higher frequency and the lower amplitude of vibration of the tube are a good occasion for reducing fatigue damage. In other words, the higher fatigue life of the tube bundles should be expected within the high void fraction conditions.

In addition, a comparison of the fatigue damages between the 7th, 20th, and 30th nodes for the five void fraction conditions was illustrated in Fig. 27. It is interesting to note that for low void fraction conditions ($\beta = 0\%$ and 20% void fraction), the fatigue damage of the 7th node is larger than those of the 20th and 30th nodes. With increasing of the void fraction, the location of the maximum fatigue damage changes. For the high void fraction conditions ($\beta = 60\%$ and 80% void fraction), the fatigue damages of the 20th and 30th nodes are larger than the one of the 7th node.

The reason for this phenomenon is that the interaction between the tube and support structure is much more obvious for the low void fraction condition, as shown in Fig. 5~Fig. 6. The clearance restriction may provide an effective support which can called as "support-active". The support structure can be seen as a hinge joint, resulting the RMS stress at 7th node is larger than the one at 30th node, as shown in Fig. 11 and Fig. 14, respectively. Nevertheless, for high void fraction conditions, a few gentle collisions between the tube and support structure can be observed in Fig. 7~Fig. 9. In other words, the support structure does not provide an effective support

which can be called as “support-inative”. The greatest RMS stress is found at the 30th node, as shown in Fig. 17, Fig. 20, and Fig. 23. This demonstrates that the clearance restriction has a significant influence on the location of the maximum fatigue damage of the tube system.

5. Conclusion

The flow-induced vibration fatigue damage of a flexible tube in a rotated triangular tube array subjected to the two-phase flow and the clearance restriction was studied based on *S-N* curves. A fatigue damage evaluation of the tube bundles was made using the time history of the stress response considering the effects of the turbulence random force and the fluidelastic force. The concluding remarks are as follows.

(1) For the tube bundles with a clearance restriction, the gap between the tube and the support structure is an important factor to estimate the fatigue damage of the tube bundles. Once the amplitude of the flow-induced vibration is larger than the gap between the tube and the TSP, the collision between the tube bundles and the TSP occurs, the fatigue life may be reduced significantly. And, the clearance restriction has a significant influence on the location of the maximum fatigue damage of the tube bundles.
(2) The void fraction of the two-phase flow has an obvious effect on the fatigue damage of the tube bundles. At the same flow pitch velocity condition, the fatigue lift of the tube within the high void fraction is greater than the tube in the low void fraction.
(3) The flow pitch velocity of the two-phase flow is a key parameter to influence the fatigue damage of the tube bundles. The fatigue damage of the tube increasing monotonously with the increasing of the flow pitch velocity in a certain void fraction condition.

CRediT authorship contribution statement

Jiang Lai: Conceptualization, Funding acquisition, Investigation. **Shihao Yang:** Writing – original draft. **Lingling Lu:** Methodology, Writing – review & editing. **Tiancai Tan:** Validation. **Lei Sun:** Supervision.

Declaration of Competing Interest

The authors declare that they have no known competing financial interests or personal relationships that could have appeared to influence the work reported in this paper.

Acknowledgments

This work was supported by the National Natural Science Foundation of China: [Grant Number 12072336].

References

[1] H. Tanaka, S. Takahara, Fluid elastic vibration of tube array in cross flow, J. Sound Vib. 77 (1) (1981) 19–37.
[2] J.H. Lever, D.S. Weaver, A theoretical model for fluidelastic instability in heat exchanger tube bundles, J. Pressure Vessel Technol. 104 (1982) 147–158.
[3] M.P. Paidoussis, D. Mavriplis, S.J. Price, A potential-flow theory for the dynamics of cylinder arrays in cross-flow, J. Fluid Mech. 146 (1984) 227–252.
[4] S.J. Price, M.P. Paidoussis, An improved mathematical model for the stability of cylinder rows subject to cross-flow, J. Sound Vib. 97 (4) (1984) 615–640.
[5] M.P. Paidoussis, S.J. Price, D. Mavriplis, A semipotential flow theory for the dynamics of cylinder arrays in cross flow, J. Fluids Eng. 107 (1985) 500–506.
[6] C.E. Taylor, M.J. Pettigrew, I.G. Currie, Random excitation forces in tube bundles subjected to two-phase cross-flow, J. Pressure Vessel Technol. 118 (1996) 265–277.
[7] E. DE LANGRE, B. VILLARD, An upper bound on random buffeting forces caused by two-phase flows across tubes, J. Fluids Struct. 12 (8) (1998) 1005–1023.
[8] C.E. Taylor, M.J. Pettigrew, Random excitation forces in heat exchanger tube bundles, J. Pressure Vessel Technol. 122 (2000) 509–514.
[9] C. Zhang, M.J. Pettigrew, N.W. Mureithi, Vibration excitation force measurements in a rotated triangular tube bundle subjected to two-phase cross flow, J. Pressure Vessel Technol. 129 (2007) 21–27.
[10] W. Xu, S. Zhang, Y. Ma, B. Liu, Fluid forces acting on three and four long side-by-side flexible cylinders undergoing flow-induced vibration (FIV), Marine Structure 75 (2021) 102877, https://doi.org/10.1016/j.marstruc.2020.102877.
[11] W. Xu, S. Zhang, Y. Ma, B. Liu, J. Wang, A study on the FIV hydrodynamic force coefficients of two staggered flexible cylinders via an inverse method, Ocean Eng. 219 (2021) 108272, https://doi.org/10.1016/j.oceaneng.2020.108272.
[12] B. de Pedro, J. Parrondo, C. Meskell, J.F. Oro, CFD modelling of the cross-flow through normal triangular tube arrays with one tube undergoing forced vibrations or fluidelastic instability, J. Fluids Struct. 64 (2016) 67–86.
[13] J. Parrondo, B. de Pedro, J. Fernández-Oro, E. Blanco-Marigorta, A CFD study on the fluctuating flow field across a parallel triangular array with one tube oscillating transversely, J. Fluids Struct. 76 (2018) 411–430.
[14] J. Lai, D. Zhang, L. Sun, L. Gao, T. Tan, P. Li, Investigation on fluidelastic instability of tube bundles considering the effect of slip ratio of air-water two-phase flow, Ann. Nucl. Energy 144 (2020) 107530, https://doi.org/10.1016/j.anucene.2020.107530.
[15] J. Lai, T. Tan, S. Yang, L. Lu, L. Sun, H. Ming, Flow-induced vibration of tube bundles considering the effect of periodic fluid force in a rotated triangular tube array, Ann. Nucl. Energy 161 (2021) 108488, https://doi.org/10.1016/j.anucene.2021.108488.
[16] M. Rottmann, K. Popp, Influence of upstream turbulence on the fluidelastic instability of a parallel triangular tube bundle, J. Fluids Struct. 18 (5) (2003) 595–612.
[17] P.A. Feenstra, D.S. Weaver, T. Nakamura, Vortex shedding and fluidelastic instability in a normal square tube array excited by two-phase cross-flow, J. Fluids Struct. 17 (6) (2003) 793–811.
[18] H.J. Chung, I.C. Chu, Fluidelastic instability of rotated square tube array in an air-water two-phase cross-flow, Nuclear Engineering and Technology 38 (1) (2006) 69–80.
[19] J. Mahon, C. Meskell, Investigation of the underlying cause of the interaction between acoustic resonance and fluidelastic instability in normal triangular tube arrays, J. Sound Vib. 324 (1-2) (2009) 91–106.

[20] W. Zhao, F. Xue, G. Shu, M. Liu, L. Lin, Z. Wang, Z. Xiao, Analysis of flow-induced vibration of steam generator tubes subjected to cross flow, Nucl. Eng. Des. 275 (2014) 375–381.
[21] B. de Pedro Palomar, C. Meskell, Sensitivity of the damping controlled fluidelastic instability threshold to mass ratio, pitch ratio and Reynolds number in normal triangular arrays, Nucl. Eng. Des. 331 (2018) 32–40.
[22] J. Lai, L. Sun, P. Li, T. Tan, L. Gao, Z. Xi, C. He, H. Liu, Eigenvalue analysis on fluidelastic instability of a rotated triangular tube array considering the effects of two-phase flow, J. Sound Vib. 439 (2019) 194–207.
[23] J. Lai, Analysis on streamwise fluidelastic instability of rotated triangular tube arrays subjected to two-phase flow, Mech. Syst. Sig. Process. 123 (2019) 192–205.
[24] J. Lai, C. He, L. Sun, T. Tan, Theoretical and experimental study on the fluidelastic instability of tube bundles in two-phase cross flow, Int. J. Press. Vessels Pip. 181 (2020) 104069, https://doi.org/10.1016/j.ijpvp.2020.104069.
[25] J. Lai, L. Sun, L. Gao, P. Li, T. Tan, Theoretical investigation of fluidelastic instability of a rotated triangular tube array in two-phase flow, Arch. Appl. Mech. 90 (10) (2020) 2347–2362, https://doi.org/10.1007/s00419-020-01725-z.
[26] J. Lai, L. Sun, P. Li, Two-phase flow-induced instability and nonlinear dynamics of a single tube in tube bundles in the transverse direction, European Journal of Mechanics / A Solids 78 (2019) 103858, https://doi.org/10.1016/j.euromechsol.2019.103858.
[27] J. Lai, L. Sun, L. Gao, T. Tan, P. Li, Two-phase flow-induced instability and nonlinear dynamics of a rotated triangular tube array in parallel direction, European Journal of Mechanics / A Solids 83 (2020) 104024, https://doi.org/10.1016/j.euromechsol.2020.104024.
[28] J. Lai, H. Wu, L. Sun, L. Gao, P. Li, Numerical investigation on Hopf bifurcation and post-instability of tube bundles subjected to two-phase cross-flow and loose support, Ann. Nucl. Energy 143 (2020) 107459, https://doi.org/10.1016/j.anucene.2020.107459.
[29] F. Axisa, J. Antunes, B. Villard, Random excitation of heat exchanger tubes by cross-flow, J. Fluids Struct. 4 (1990) 321–341.
[30] M.P. Paidoussis, G.X. Li, R.H. Rand, Chaotic motions of a constrained pipe conveying fluid: Comparison between simulation, analysis, and experiment, J. Appl. Mech. 58 (1991) 559–565.
[31] M.P. Paidoussis, C. Semler, Nonlinear and chaotic oscillations of a constrained cantilevered pipe conveying fluid: A full nonlinear analysis, Nonlinear Dyn. 4 (6) (1993) 655–670.
[32] M.A. Miner, Cumulative damage in fatigue, J. Appl. Mech. 3 (1945) 159–164.
[33] J. Tan, Corrosion fatigue behavior of nuclear-grade austenitic alloys in high temperature and high pressure water, Ph. D dissertation, University of Science and Technology of China, 2015.